Experimental measurements of static pressure ahead of normal surface

Figure 2 presents experimental measurements of the static pressure ahead of the normal surface for four different nozzle-to-normal-surface spacings. In Fig. 2 experimental data ahead of the normal surface are superimposed on static pressure experimental data without the normal surface in the freejet flowfield. The distance of influence ahead of the normal surface is obtained directly from these experimental data. This extent of influence is referred to as the standoff distance. Figure 3 presents the standoff experimental results vs Y/D position of the normal surface. Two distinct regions of standoff exist in Fig. 3. A percent standoff of approximately 28% exists for freejet impingement onto the normal surface while for close nozzle-to-normal-surface spacing the Coanda effect generates a rather linear increase in percent standoff with decrease in Y/D position. Figure 3 also presents experimental data related to the lateral limit of jet influence on the normal surface. This lateral limit of influence is taken as the point on the normal surface where the static pressure is equal to the atmospheric pressure. Two values exist for the lateral jet influence at $Y/D = 4.31$ due to the existence of the base region Coanda effect.

Conclusions

The standoff distance experimental results presented in Fig. 3 deviate from Shauer and Eustis[6] theory by approximately 3%. This is not surprising as the Shauer and Eustis theory was developed for incompressible flow. Wolfshtein[7] assumed a value of 33% for standoff in his incompressible model of the impingement region. This value deviates from these experimental data by approximately 5%. A standoff percentage of approximately 28% is indicated for Y/D positions greater than 35. A more detailed presentation and discussion of the results related to this experimental investigation may be found in Ref. 11.

References

[1] Poreh, M. and Cernak, J. E., "Flow Characteristics of a Circular Submerged Jet Impinging Normally on a Smooth Boundary," *Proceedings of the Sixth Midwestern Conference on Fluid Mechanics*, Vol. 6, Univ. of Texas, Austin, 1959, pp. 198–212.

[2] Tomich, J. F., "Heat and Momentum Transfer from Compressible Turbulent Jets of Hot Air Impinging Normally on a Surface," Ph.D. dissertation, 1967, Sever Inst. of Technology, Washington Univ., St. Louis, Mo.

[3] Kim, T. S., "Analysis of Flow Characteristics in Circular, Submerged, Impinging Jets," Ph.D. dissertation, 1967, Mechanical Engineering Dept., Illinois Inst. of Technology, Chicago, Ill.

[4] Vickers, J. M., "Heat Transfer Coefficients Between Fluid Jets and Normal Surfaces," *Industrial Engineering Chemistry*, Vol. 51, No. 8, June 1959, pp. 967–972.

[5] Rudov, I. M. and Uskov, V. N., "Approximate Method of Calculating the Parameters of a Supersonic Jet Impinging on an Inclined Plane Barrier," *Aviatsionnaia Tekhnika*, Vol. II, No. 3, Dec. 1968, pp. 79–84.

[6] Shauer, J. J. and Eustis, R. H., "The Flow Development and Heat Transfer Characteristics of Plane Turbulent Impinging Jets," TR3, Oct. 1963, Mechanical Engineering Dept., Stanford Univ., Stanford, Calif.

[7] Wolfshtein, M., "Convection Processes in Turbulent Impinging Jets," Rept. SF/R/2, Nov. 1967, Mechanical Engineering Dept., Imperial College of Science and Technology, London, England.

[8] Volluz, R. J., *Handbook of Supersonic Aerodynamics-Wind Tunnel Instrumentation and Operation*, NAVORD Rept. 1488, Vol. 6, Bureau of Naval Weapons, Oct. 1961.

[9] Rayle, R. E., "An Investigation of the Influence of Orifice Geometry on Static Pressure Measurements," M.S. thesis, 1949, Mechanics Dept., MIT, Cambridge, Mass.

[10] Kirshner, J. M., "Introduction to Fluidics," *Fluidics Quarterly*, Vol. 2, Feb. 1968, pp. 93–102.

[11] Knight, C. V., "A Study of the Impingement on a Normal Surface of Flow Emanating from Two-Dimensional, Supersonic, Air Nozzles," Ph.D. dissertation, 1971, Mechanical and Aerospace Engineering Dept., Univ. of Tennessee, Knoxville, Tenn.

Finite Deflection of a Deep Arch with Boundary Imperfections

ARUP CHATTOPADHYAY* AND GURBACHAN DHATT†

Civil Engineering Department, Laval University, Quebec

THE nonlinear behavior of deep arches has recently received considerable attention. Huddleston,[1] DaDeppo and Schmidt,[2] and Sharifi and Popov[3] have applied various techniques to study the finite deflection behavior of these structures. However, the effects of imperfect boundary conditions on the buckling loads do not seem to have been studied except by Bolotin.[4] The purpose of this Note is to analyze the nonlinear symmetrical and unsymmetrical buckling of deep arches with symmetrical boundary imperfections which are simulated by attaching a rotational spring at the support. The spring stiffness is varied to obtain the hinged, clamped, or intermediate boundary conditions. The experience obtained by studying this buckling phenomena can be usefully employed for the analysis of deep shells which is presently under way.

Formulation

The displacements $\bar{u}$ and $\bar{w}$ of a point of arch are defined along the surface coordinates s and z, respectively (Fig. 1). The strain displacement relations for thin arches are specialized as follows:

$$e_m = \partial\bar{u}/\partial s + \bar{w}/R + \beta^2/2; \quad e_b = \zeta\,\partial\beta/\partial s;$$

and

$$\beta = \bar{u}/R - \partial\bar{w}/\partial s \tag{1}$$

The total potential energy is

$$\pi = \int_s (U - \lambda p\bar{w})\,ds + \tfrac{1}{2}\Sigma(\bar{K}_i B_i^2) \tag{2}$$

and

$$U = (Eh/2)e_m^2 + (Eh^3/24)(\partial\beta/\partial s)^2 \tag{3}$$

p is the applied normal load and λ is the magnitude factor. The imperfect boundary constraints are introduced by the spring mechanism represented by the last term in Eq. (2). $\bar{K}_i$ is the rotational spring stiffness and β_i is the rotation at a point s_i of the arch. The summation sign indicates the possibility of various rotational springs along the center line of the arch.

The displacements $\bar{u}$ and $\bar{w}$ over an element are each approximated by a cubic polynomial. The element stiffness matrix (8×8) and the consistent load vector are obtained in a routine manner by minimizing π in Eq. (2). The resulting nonlinear equations are solved by the Newton-Raphson method with a modification for changing the role of dependent and independent variables. The unsymmetrical bifurcations for symmetrical loading (if it exists) are initiated by giving a finite perturbation to the zero value of the slope at the symmetry point of the complete arch. The complete unsymmetric path may then be traced by the Newton-Raphson technique. The details of the numerical method are given in Refs. 5 and 6.

Illustrative Examples

For convenience, the results in this section are presented in nondimensional form in terms of the following parameters:

$$\mu = \Theta^2 R/h; \quad Q = -(12\Theta^2 R^3 p)/\pi^2 Eh^3; \quad (u, w) = -(\bar{u}, \bar{w})/\Theta^2 R \tag{4}$$

$$\bar{K} = K/1 - K; \quad f = Q_{cr}(K)/Q_{cr}(K = 1); \quad H_c = -(e_m)_{s=0}$$

Received May 12, 1972; revision received September 25, 1972. This research is partially supported by NRC Grant/1593.

Index category: Structural Stability Analysis.

* Postdoctoral Fellow.

† Assistant Professor.

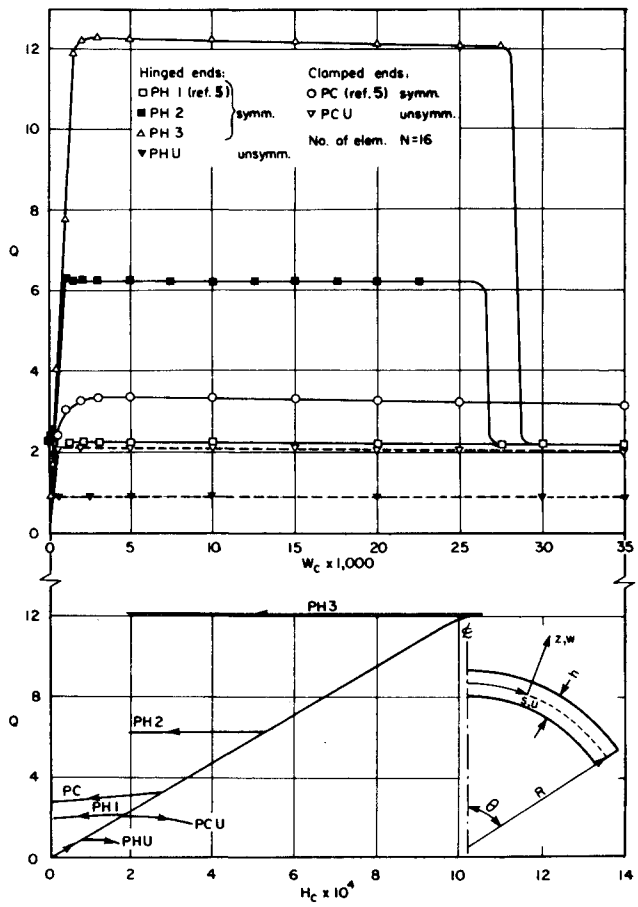

Fig. 1 Buckling of deep arches.

where Θ, R, h, and E are the semiangle, radius of curvature, thickness, and modulus of elasticity, respectively. Q is the nondimensional load corresponding to the uniform normal pressure p; Q_{cr} is the critical (symmetrical or unsymmetrical) load for a given boundary constraint. The spring stiffness $\bar{K}$, varying from 0 to infinity, is represented in terms of scaled stiffness K, which varies from 0 to 1. H_c and w_c are, respectively, the non-

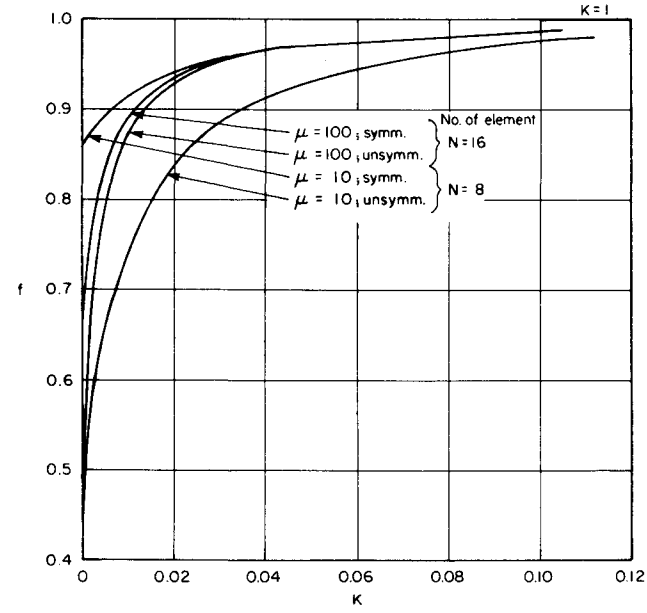

Fig. 2 Buckling loads due to boundary imperfections.

Table 1 Coefficients B, C, and $Q_{cr}(K = 1)$.

Curve	Description	B	C	$Q_{cr}(K = 1)$
1	$\mu = 100$ (symm.)	0.66522	108.76262	3.35576
2	$\mu = 100$ (unsymm.)	0.45107	181.02094	2.16179
3	$\mu = 10$ (symm.)	0.85865	36.37755	2.30526
4	$\mu = 10$ (unsymm.)	0.49071	66.28336	1.89795

dimensional axial compression and displacement w at $s = 0$. f is the critical load factor corresponding to a value of K. All the arches have unit width.

To verify the accuracy of the element, the buckling loads of a hinged circular arch with a concentrated load at the center are studied. The geometrical parameters are taken as:

$$R/h = 100; \quad h = 1; \quad Q = 0.927295(\text{rad}); \quad I = h^3/12$$

In the present study, the symmetrical critical load is obtained (with 8 elements for half the arch) as 15.48 EI/R^2, whereas, in Refs. 1 and 3, it is found as 15.23 EI/R^2 and 15.845 EI/R^2. The unsymmetrical critical load is obtained (with 16 elements for the whole arch) as 13.04 EI/R^2 and in Refs. 1, 2, and 3, it is given as 13.01 EI/R^2, 13.00 EI/R^2, and 13.036 EI/R^2. This shows that the present element is quite reliable.

The load deflection relations for a deep arch having $\mu = 100$, $R/h = 100$ under uniform normal load with hinged and clamped boundary conditions are shown in Fig. 1. The pre- and post-buckling configurations, corresponding to symmetrical snap-through and unsymmetrical bifurcations for the hinged arch, are represented by curves PH3, Ph2, Ph1, and PHU. PH1, PH2, and PH3 denote w_c vs Q curves corresponding to three different equilibrium paths for symmetrical deformations, whereas, PHU denote the same for unsymmetrical deformation. Similar relations for clamped arch are shown by curves PC (symmetrical) and PCU (unsymmetrical). Surprisingly, the configurations corresponding to PH2 and PH3 give critical loads higher than those obtained for clamped arch PC. The curves PH2 and PH3 finally coincide with the curve PH1 which gives a critical load lower than that for a clamped arch, as expected. This peculiar behavior of deep hinged arch has not been observed for shallow arches. The explanation of this behavior is still under study.

The axial compression H_c is plotted against Q in Fig. 1 corresponding to the load displacement curves shown in the same figure. It is observed that the thrust H_c decreases after symmetrical buckling, whereas it increases in case of unsymmetrical buckling for both hinged and clamped arches. The initiation of instability is observed at points of slope discontinuities in H_c vs Q curves.

The influence of intermediate boundary constraints represented by different values of K (0 to 1) on the buckling load factor f of the deep arches are shown in Fig. 2. Curves 1 and 2 give symmetrical and unsymmetrical buckling loads for an arch with $\mu = 100$, $R/h = 100$. Curve 4 gives unsymmetrical buckling loads for an arch with $\mu = 10$, $R/h = 100$. These curves may be approximated analytically with less than 5% error by the relation

$$f = 1 + (B - 1)\, e^{-C\bar{K}} \tag{5}$$

The values of B and C and the buckling load for the clamped arch, $Q_{cr}(K = 1$ or $\bar{K} = \infty)$ are given in Table 1.

The relation [Eq. (5)] may be usefully employed to obtain the probabilistic buckling loads due to given probability distributions for boundary imperfections. For example, if $P(\bar{K})$ is the probability density for $\bar{K}$, the probability density for f is given by[4]

$$P(f) = P(\bar{K})/(df/d\bar{K}) \tag{6}$$

Concluding Remarks

Deep strain displacement relations should be employed for nonlinear analysis of deep arches by the finite element method. Different symmetrical equilibrium paths PH1, PH2, PH3 are obtained for deep hinged arch which are not observed in

shallow arches. The Q vs w_c curves remain almost flat for deep arches in the initial post-buckling region. However, the magnitude of w_c still remains very small. The buckling load is very sensitive to imperfections in hinged conditions and is almost insensitive to realistic clamped imperfections. A probabilistic estimate of buckling loads may be made by using the results of Fig. 2 and the expression (6) for a given probability density of boundary imperfections.

References

[1] Huddleston, J. V., "Finite Deflection and Snap-Through of High Circular Arches," *Journal of Applied Mechanics*, Vol. 35, No. 4, Dec. 1968, pp. 763–769.

[2] DaDeppo, D. A. and Schmidt, R., "Sidesway Buckling of Deep Circular Arches under a Concentrated Load," *Journal of Applied Mechanics*, Vol. 36, No. 2, June 1969, pp. 325–329.

[3] Sharifi, P. and Popov, E. P., "Nonlinear Buckling Analysis of Sandwich Arches," *Journal of the Engineering Mechanics Division*, ASCE, Vol. 97, No. EM5, Oct. 1971, pp. 1397–1412.

[4] Bolotin, V. V., *Statistical Methods in Structural Mechanics*, Holden-day, San Francisco, 1969.

[5] Chattopadhyay, A. and Dhatt, G., "Probabilistic Buckling of Curved Structures with Imperfect Boundary Conditions," *Proceedings of the Symposium on the Finite Element Method in Civil Engineering*, Engineering Inst. of Canada, June 1972, pp. 303–324.

[6] Dhatt, G. S., "Instability of Thin Shells by the Finite Element Method," *Symposium on International Association of Shell Structures*, Vienna, Sept. 1970.

Variation of the Van Driest Damping Parameter with Mass Transfer

TUNCER CEBECI*

California State University, Long Beach, Calif.

Introduction

CURRENTLY there are several prediction methods based on the eddy viscosity concept for calculating turbulent boundary layers. In these methods the boundary layer is regarded as a composite layer consisting of inner and outer regions and separate expressions are used for eddy viscosity in each region. A popular eddy viscosity expression for the inner region is based on Prandtl's mixing length theory with a modification suggested by Van Driest,[1] namely,

$$\varepsilon = (\kappa y)^2[1-\exp(-y/A)]^2|\partial u/\partial y| = L^2|\partial u/\partial y| \tag{1}$$

where

$$L = \kappa y[1-\exp(-y/A)] \tag{2a}$$

$$A = A^+\nu(\tau_w/\rho)^{-1/2} \tag{2b}$$

and A^+ is an empirical constant equal to 26.

The outer viscosity formula is

$$\varepsilon = \alpha u_e \delta_k^* \tag{3}$$

The right-hand side of (3) is sometimes multiplied by Klebanoff's intermittency factor[2] γ to account for the intermittent character of the turbulent boundary layer. In (3), δ_k^* is a kinematic displacement thickness given by

$$\delta_k^* = \int_0^\infty \left(1-\frac{u}{u_e}\right)dy$$

Commonly accepted values for κ and α vary between 0.40–0.41 and 0.016–0.0168, respectively. With these constants the above eddy-viscosity distribution fits well to the incompressible flat-plate data of Klebanoff,[2] and provides good agreement with experiment when used in the solution of the boundary layer equations. On the other hand, when the same eddy-viscosity formulation is used to calculate turbulent boundary layers with mass transfer, calculations show poor agreement with experiment and indicate the need for modification of the formulation.

Most of the attempts made to modify (1) and (3) for mass transfer accept the universality of the parameters κ and α in (1) and in (3) and choose to adjust or modify only (2) in (1). A recent study[3] conducted by the present author shows that while κ is a universal constant, α is not, and that at low Reynolds numbers α varies with Reynolds number. However, in the present study we restrict our attention to (2) and discuss its modification to account for the mass transfer.

Variation of the Van Driest Damping Parameter A^+ with Mass Transfer Velocity v_w^+

Consider an incompressible turbulent flow over a porous flat-plate. The momentum equation is

$$u(\partial u/\partial x)+v(\partial u/\partial y) = (1/\rho)(\partial\tau/\partial y) \tag{4}$$

where $\tau = \tau_l+\tau_t = \mu(\partial u/\partial y)-\rho\langle u'v'\rangle$. Close to the wall u is small so that the first term can be neglected. Equation (4) then becomes

$$v_w(du/dy) = (1/\rho)(d\tau/dy) \tag{5}$$

Integration of that equation and use of the boundary conditions $\tau(0)=\tau_w$, $u(0)=0$, and the introduction of dimensionless quantities $u^+ = u/u_\tau$ and $v_w^+ = u/u_\tau$ allows the resulting expression to be written as

$$\tau/\rho u_\tau^2 = 1+v_w^+u^+ \tag{6}$$

Using the definition of eddy viscosity and the expression given by (1), we can also write

$$\tau/\rho u_\tau^2 = 1/u_\tau^2[\nu(du/dy)+L^2(du/dy)^2] \tag{7}$$

With the use of (7), we can write (6) as

$$(L^+)^2(du^+/dy^+)^2+du^+/dy^+-(1+v_w^+u^+) = 0 \tag{8}$$

where

$$L^+ = \kappa y^+[1-\exp(-y^+/A^+)] \tag{9}$$

Before (8) can be solved it is necessary to know v_w^+ and A^+. Since $v_w^+ = (v_w/u_e)(2/c_f)^{1/2}$, we can determine v_w^+ for a specified v_w/u_e provided that c_f is known. Here we obtain c_f from the law of the wall and the law of the wake expression of Coles[4] generalized

$$u_p^+ = (1/\kappa)\ln y^+ + c + (\Pi/\kappa)w(y/\delta) \tag{10}$$

where

$$u_p^+ = \frac{2}{v_w^+}[(1+v_w^+u^+)^{1/2}-1]$$

$$c = c_o+\frac{2}{v_w^+}[(1+Kv_w^+)^{1/2}-1]-K \tag{11}$$

According to Coles's recent paper,[4] Eq. (10) fits the available experimental data very well. As in flows with no mass transfer, for zero pressure gradient flows, the profile parameter Π is a function of Reynolds number for values of $R_\theta < 5000$. The parameters c_o and K in (11) are universal constants with values of 5.0 and 10.805, respectively. It can be shown that for zero mass transfer, (10) reduces to Coles's previous expression, that is

$$u^+ = (1/\kappa)\ln y^+ + c_o + (\Pi/\kappa)w(y/\delta)$$

To obtain the local skin-friction coefficient from (10), we evaluate that expression at $y=\delta$; this gives

$$2z/\bar{v}_w[(1+\bar{v}_w z^2)^{1/2}-1] = (1/\kappa)\ln\delta^+ + c + 2\Pi/\kappa \tag{12}$$

where $\bar{v}_w = v_w/u_e$, $z = (2/c_f)^{1/2}$, $\delta^+ = \delta u_e/\nu$.

Received May 15, 1972; revision received August 17, 1972. This work was supported by National Science Foundation Grant GK-30981.

Index category: Boundary Layers and Convective Heat Transfer—Turbulent.

* Adjunct Professor, Mechanical Engineering Department. Member AIAA.